

Generation of Optical Skyrmions with Tunable Topological Textures

Yijie Shen,* Eduardo Casas Martínez, and Carmelo Rosales-Guzmán*


Cite This: *ACS Photonics* 2022, 9, 296–303


Read Online

ACCESS |

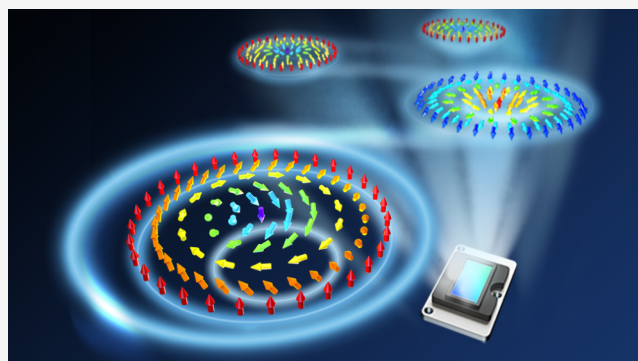
Metrics & More

Article Recommendations

Supporting Information

ABSTRACT: In recent times, the optical-analogous skyrmions, topological quasiparticles with sophisticated vectorial structures in light, have received an increasing amount of interest. Here we propose theoretically and experimentally a generalized family of these, the tunable optical skyrmions, unveiling a new mechanism to transform between various skyrmionic topologies, including Néel, Bloch, and antiskyrmion types, via simple parametric tuning. In addition, a geometric Skyrme–Poincaré representation is proposed to visualize the complete topological evolution of tunable skyrmions, which we term the skyrmion torus. To generate the tunable optical skyrmions experimentally, we implemented a digital hologram system based on a spatial light modulator, the results of which show great agreement with our theoretical predictions.

KEYWORDS: skyrmion, topology, structured light, vector beams, spatial light modulator, orbital angular momentum



Skyrmions are topologically protected quasiparticles in high-energy physics and condensed matter with salient vectorial textures.^{1,2} This concept was recently identified by the optics and photonics community as a cutting-edge topic. Recently, skyrmions were constructed in optical fields as state-of-the-art optical structures and termed optical skyrmions.³ These were first generated in the electric field of evanescent waves,³ followed by diverse forms constructed from different kinds of optical fields, such as spin fields of confined free-space waves,^{4,5} Stokes vectors of paraxial vector beams,^{6,7} magnetic vectors in propagating light pulses,⁸ and pseudospins in photonic crystals.⁹ The creation of optical skyrmions has promising advanced applications in fields such as nanoscale metrology,¹⁰ deep-subwavelength microscopy,⁴ ultrafast vector imaging,¹¹ and topological Hall devices,⁹ broadening the frontier of modern fundamental and applied physics.

The advancement that skyrmions provide is mainly in their versatile topological textures, providing new degrees of freedom to shape vectorial fields and encode information. The skyrmionic configuration can be mapped into real-space magnetic materials and classified into diverse topologies,^{12,13} including Néel type,¹⁴ Bloch type,¹⁵ and antiskyrmion.¹⁶ However, control of the diverse topologies of optical skyrmions is an emerging topic that is still in its infancy. As the first scheme of optical skyrmions, the evanescent electric fields on a plasmonic surface can form only Néel-type skyrmions.^{3,11} One year ago, a study of plasmonic skyrmions controlled between the Néel and Bloch types was reported,¹⁷ but soon after, such Bloch-type skyrmions were disproved.^{18,19} The loophole-free observation of Bloch-type optical skyrmions was reported very recently in optical chiral multilayers.²⁰ For

optical skyrmions in free space, a Bloch-type skyrmion was proved in the spin field of a tightly focused vortex beam.⁴ Soon after, both Néel- and Bloch-type skyrmions were theoretically presented in Stokes vectors of paraxial vector beams⁶ and electric–spin fields in tightly focused vector beams.⁵ It is also of great importance to explore intermediate skyrmion-like states with extended topology, such as intermediate states between meron (half-charge skyrmion) and skyrmion in magnets^{21,22} and light.^{10,23} However, no experimental results have been reported for skyrmions with tunable topological textures in free space. Also, the concept of optical antiskyrmions has not yet been realized.

In this paper, a closed-form expression is proposed to characterize a general class of optical skyrmions, where skyrmions with different textures (Néel, Bloch, and anti-skyrmion types) can be topologically transformed among each other via simple parametric tuning. Moreover, a novel geometrical model, the skyrmion torus, is proposed to universally map the topological transformations of tunable optical skyrmions. Importantly, we experimentally generated the tunable optical skyrmions with all of the topological types in structured vector beams controlled by a digital hologram system, showing great agreement with the theoretical predictions.

Received: November 4, 2021

Published: January 4, 2022



ACS Publications

© 2022 American Chemical Society

THEORY

Topologies of Skyrmions. The topological properties of a skyrmionic configuration can be characterized by the skyrmion number, defined as¹³

$$s = \frac{1}{4\pi} \iint_{\sigma} \mathbf{n} \cdot \left(\frac{\partial \mathbf{n}}{\partial x} \times \frac{\partial \mathbf{n}}{\partial y} \right) dx dy \quad (1)$$

where $\mathbf{n}(x, y)$ represents the vector field to construct a skyrmion and σ denotes the region to confine the skyrmion, which can be infinity (for an isolated skyrmion) or a cell of a periodic distribution (for skyrmion lattices). The skyrmion number is an integer that counts how many times the vector $\mathbf{n}(x, y) = \mathbf{n}(r \cos \theta, r \sin \theta)$ wraps around the unit sphere, as shown by the mapping in Figure 1a. For mapping to the unit sphere, the vector can be given by $\mathbf{n} = (\cos \alpha(\theta) \sin \beta(r), \sin \alpha(\theta) \sin \beta(r), \cos \beta(r))$. Also, the skyrmion number can be separated into two integers:

$$\begin{aligned} s &= \frac{1}{4\pi} \int_0^{r_\sigma} dr \int_0^{2\pi} d\theta \frac{d\beta(r)}{dr} \frac{d\alpha(\theta)}{d\theta} \sin \beta(r) \\ &= \frac{1}{4\pi} [\cos \beta(r)]_{r=0}^{r_\sigma} [\alpha(\theta)]_{\theta=0}^{\theta=2\pi} \\ &= q \cdot m \end{aligned} \quad (2)$$

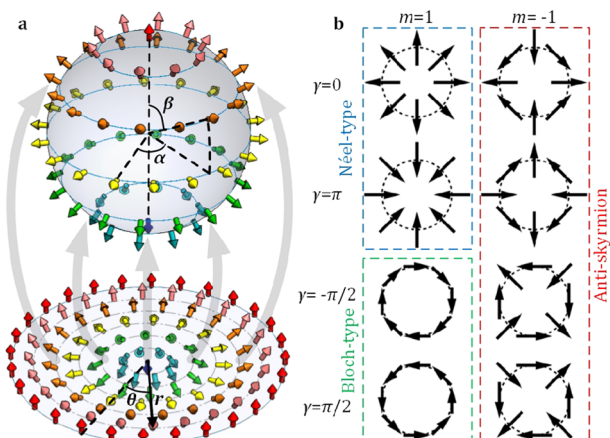


Figure 1. (a) Mapping from a normal skyrmion configuration, constructed by the colored arrows, to the unit sphere representation. (b) Some basic cases of the transversely projected vector (components E_x and E_y) distribution at given radii of the skyrmions with various values of m and γ .

in which the polarity $q = \frac{1}{2}[\cos \beta(r)]_{r=0}^{r_\sigma}$ indicates the direction of the vector [down (up) at the center $r = 0$ and up (down) at the boundary $r \rightarrow r_\sigma$ for $q = 1$ ($q = -1$)] and the vorticity $m = \frac{1}{2\pi}[\alpha(\theta)]_{\theta=0}^{\theta=2\pi}$ controls the distribution of the transverse field components.²⁴ In the case of a helical distribution, an initial phase γ should be added: $\alpha(\theta) = m\theta + \gamma$. If we consider the transverse vector components at a given radius (or a given latitude angle β in the unit-sphere representation), γ reveals the inclined angle of the initial vector in the circular array (see Figure 1b). For the $m = 1$ skyrmion, the cases of $\gamma = 0$ and $\gamma = \pi$ are classified as Néel type, and the cases of $\gamma = \pm\pi/2$ are Bloch type. The case of $m = -1$ is antiskyrmion.

Tunable Optical Skyrmions. In order to derive a closed-form expression that allows tuning between optical skyrmions with diverse topological textures via simple parameters, we start with a classical model of the optical skyrmion, which was also the first model of an optical skyrmion. In this model, the skyrmionic vector field $\mathbf{n} = (n_x, n_y, n_z)$ is constructed from the electric field vectors $(E_x, E_y, E_z)^T / |\mathbf{E}|$, in a confined surface plasmon polariton (SPP) wave:³

$$\mathbf{n} = E_0 e^{-ik_z z} \sum_{n=1}^N \begin{cases} -\frac{|k_z| \cos \theta_n}{k_{||}} \sin(k_{||} \mathbf{r}_{||} \cdot \boldsymbol{\theta}_n) \\ -\frac{|k_z| \sin \theta_n}{k_{||}} \sin(k_{||} \mathbf{r}_{||} \cdot \boldsymbol{\theta}_n) \\ \cos(k_{||} \mathbf{r}_{||} \cdot \boldsymbol{\theta}_n) \end{cases} \quad (3)$$

where E_0 is a normalized amplitude, $k_{||}$ and k_z are the transverse (in-plane) and axial wavenumbers, respectively, $\mathbf{r}_{||} = (x, y)$, and $\boldsymbol{\theta}_n = (\cos \theta_n, \sin \theta_n)$. The physical meaning of eq 3 is the superposition of N standing-wave SPPs along directions with equally distributed in-plane angles θ_n ($n = 1, 2, \dots, N$). For common circular-shaped skyrmions, N should be large enough, ideally $N \rightarrow \infty$. For the case of a skyrmion lattice, N should be an integer related to the boundary geometry, e.g., $N = 3$ is set to simulate a hexagonal skyrmion lattice field with $\theta_n = [-\pi/3, 0, \pi/3]$.³ Figure 2a shows simulated results for a skyrmionic vector distribution that were obtained using eq 3. However, eq 3 can only represent Néel-type skyrmions (lattice). Here we propose a mathematically generalized form that breaks this limit:

$$\mathbf{n} = E_0 e^{-ik_z z} \sum_{n=1}^N \begin{cases} -\frac{|k_z| \cos(\theta_n + \phi_1)}{k_{||}} \sin(k_{||} \mathbf{r}_{||} \cdot \boldsymbol{\theta}_n) \\ -\frac{|k_z| \sin(\theta_n + \phi_2)}{k_{||}} \sin(k_{||} \mathbf{r}_{||} \cdot \boldsymbol{\theta}_n) \\ \cos(k_{||} \mathbf{r}_{||} \cdot \boldsymbol{\theta}_n) \end{cases} \quad (4)$$

Compared with eq 3, eq 4 has two additional parameters, ϕ_1 and ϕ_2 , the control of which can drive the skyrmionic vector field to cover all three classic types of topologies: Néel type for $\phi_1 = \phi_2 = 0$ or $\phi_1 = \phi_2 = \pi$, Bloch type for $\phi_1 = \phi_2 = \pi/2$ or $\phi_1 = \phi_2 = 3\pi/2$, and antiskyrmion for $|\phi_1 - \phi_2| = \pi$. Numerically simulated results obtained using eq 4 for these three topological types are shown in Figure 2a–c. In general, ϕ_1 and ϕ_2 act as the parameters to dynamically tune the topological textures among the three typical ones.

It is worth noting that the Néel-type texture can continuously deform into the Bloch-type texture. In general, the intermediate skyrmions can be interpreted using eq 4 with $\phi_1 = \phi_2 = \phi \in [0, 2\pi]$ ($\phi = 0, \pi$ for Néel type and $\phi = \pi/2, 3\pi/2$ for Bloch type). Video S1 shows this evolution, and an example of an intermediate skyrmion is presented in Figure 2d. However, it is impossible to deform the antiskyrmion into a Néel- or Bloch-type skyrmion because they have different topological protection (opposite vorticity). When the evolution goes from a Néel-type or Bloch-type skyrmion to an antiskyrmion, the vector field must meet a boundary state of a nonskyrmion, an example of which is shown in Figure 2e. In the nonskyrmion, the transverse component vectors have only a single 45° orientation, which is why it is not a skyrmion (a

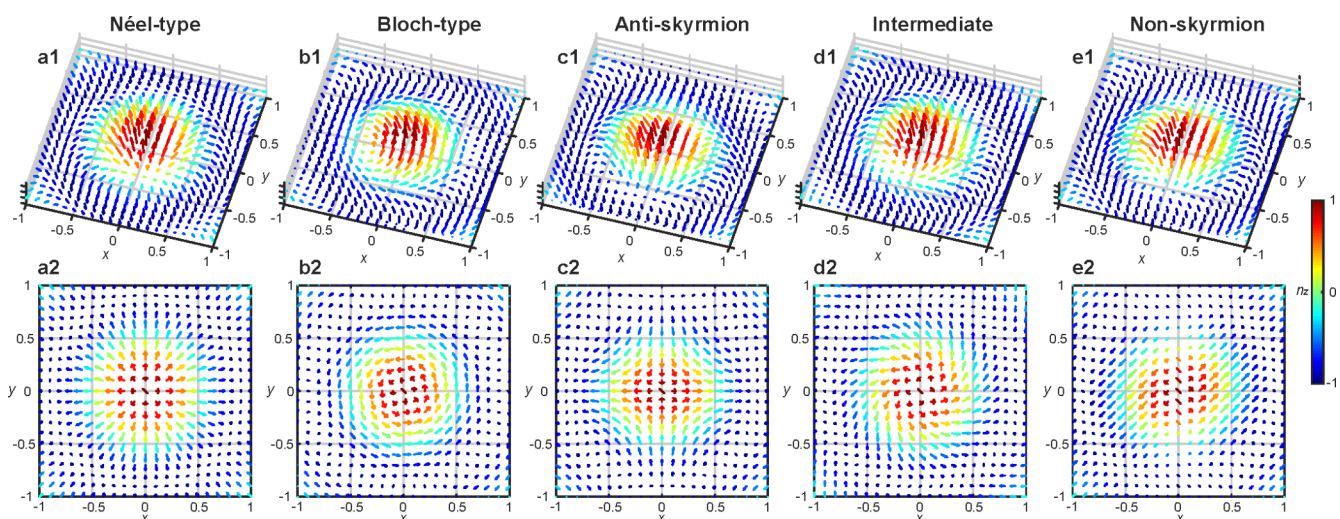


Figure 2. Simulated results for (a1–e1) the 3D vector distributions (n_x, n_y, n_z) and (a2–e2) the transverse component vectors (n_x, n_y) for (a–d) tunable optical skyrmions with diverse topological textures of (a) Néel type ($\phi_1 = \phi_2 = 0$), (b) Bloch type ($\phi_1 = \phi_2 = \pi/2$), (c) antiskyrmion ($\phi_1 = 0, \phi_2 = \pi$), and (d) an intermediate state ($\phi_1 = \phi_2 = \pi/4$) and (e) a nonskyrmion ($\phi_1 = 0, \phi_2 = \pi/2$).

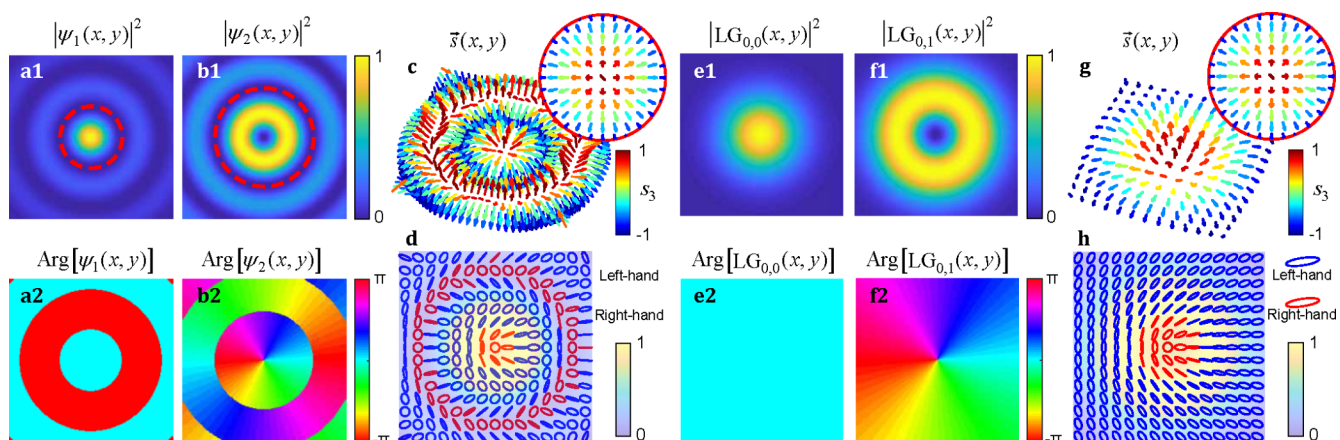


Figure 3. (a, b) Intensity (a1, b1) and phase (a2, b2) distributions of (a) $\psi_1(x, y)$ and (b) $\psi_2(x, y)$ for the case of $\phi_1 = \phi_2 = 0$. The red dashed lines mark the effective regions to induce the main topological texture of the optical skyrmion. (c) Skyrmion in a Stokes vector field with the transverse component inset and (d) the intensity and polarization distributions of the corresponding vector beam. (e, f) Intensity (e1, e2) and phase (f1, f2) distributions of (e) $LG_{0,0}(x, y)$ and (f) $LG_{0,1}(x, y)$ modes at the beam-waist plane. (g) Skyrmion in a Stokes vector field with the transverse component inset and (h) the intensity and polarization distributions of the LG-based vector beam.

skyrmion requires the transverse component to cover the full azimuth range). Video S2 (Video S3) shows the evolution from a Bloch (Néel) skyrmion to an antiskyrmion.

The mathematical representation given in eq 4 is correct for tunable optical skyrmions, but their experimental realization is still cumbersome. If one were to attempt to use SPPs to generate tunable skyrmions as described by eq 4, the two parameters ϕ_1 and ϕ_2 would induce extreme conditions that are hard to fulfill, as a stable SPP field requires more rigorous conditions than a free-space light field.

Importantly, recent advancements have made possible the successful realization of optical skyrmions of different optical vector fields in both matter and free space, but these are still limited to few topological textures.^{4–6,9} These advancements allowed us to propose a practical scheme for the generation of tunable optical skyrmions in free space via the Stokes vectors of structured vector beams. The Stokes vector $s = (s_1, s_2, s_3)$ can represent an arbitrary state of polarization as points on the surface of the unit-radius sphere known as the Poincaré sphere.²⁵ In spherical coordinates, the optical field $\psi = \cos(\theta)/$

$2) e^{-i\phi/2}R + \sin(\theta/2) e^{i\phi/2}L$, where R and L represent right-handed circularly polarized (RCP) and left-handed circularly polarized (LCP) eigenstates, respectively, is represented as $s = (\cos \varphi \sin \theta, \sin \varphi \sin \theta, \cos \theta)$. In order to construct skyrmions using the Stokes vector, we need to first construct a vector beam with customized spatial modes of the form,

$$\psi(x, y) = \psi_1(x, y)R + \psi_2(x, y)L \quad (5)$$

The spatial modes ψ_1 and ψ_2 should have the same form as the tunable skyrmion, given by eq 4, that is,

$$\psi_1(x, y) = \cos[\theta(x, y)/2] e^{-i\varphi(x, y)/2} \quad (6)$$

$$\psi_2(x, y) = \sin[\theta(x, y)/2] e^{i\varphi(x, y)/2} \quad (7)$$

with

$$\theta(x, y) = \cos^{-1}[n_z(x, y)] \quad (8)$$

$$\varphi(x, y) = \sin^{-1} \left[\frac{n_y(x, y)}{\sin \theta(x, y)} \right] = \cos^{-1} \left[\frac{n_x(x, y)}{\sin \theta(x, y)} \right] \quad (9)$$

where, (n_x, n_y, n_z) is exactly based on the theoretical tunable skyrmion given by eq 4. We can now tailor vector beams to realize tunable skyrmions via their Stokes vector fields. As an example, a numerical simulation of the Néel-type skyrmionic vector beam, for which $\phi_1 = \phi_2 = 0$, is shown in Figure 3. The spatial modes $\psi_1(x, y)$ and $\psi_2(x, y)$, which are shown in Figure 3a,b, share the same amplitude and phase distributions as the transverse zeroth- and first-order Bessel modes, respectively. It should be noted that although they share the same form, $\psi_1(x, y)$ and $\psi_2(x, y)$ are derived from surface plasma fields located on a 2D surface, whereas Bessel beams are propagating beams. The distributions of the Stokes vectors, intensities, and polarizations are shown in Figure 3c,d, respectively, where the central region of a Néel-type skyrmion texture and full states of polarization can be observed. The simulation results also show that the effective regions that contribute to the main hedgehoglike vector texture are the central lobes of the zeroth- and first-order Bessel modes, as marked by the red dashed lines in Figure 3a,b, whereas the side lobes of the Bessel beams, far away from the skyrmion center, contribute to the repeating radial reversal vector structure, which does not impact the skyrmion topology. Therefore, we can replace the zeroth- and first-order Bessel modes by the fundamental Gaussian and first-order Laguerre–Gaussian (LG) modes, i.e., $LG_{0,0}$ and $LG_{0,1}$ (Figure 3e,f). The Stokes vector field of the corresponding LG-based vector beam given by eq 5 shows a perfect Néel-type skyrmion, as evinced in Figure 3c,d. It should be noted that in contrast to the nondiffracting Bessel modes, the LG modes are diffracting beams; here we observe the skyrmions at the beam-waist plane of the beams.

Skyrmion Torus and Skyrme–Poincaré Model. In this section we present an elegant graphical model, the skyrmion torus, to depict the general topological state transformation of a tunable skyrmion onto a torus. Without loss of generality, setting $\phi_1 = \Phi \in [0, 2\pi]$ and $(\phi_2 - \phi_1) = \Theta \in [-\pi, \pi]$, we can regard Φ and Ψ as the angles of the toroidal and poloidal directions, respectively, to map the general topological states of skyrmions to the corresponding points on a torus, as shown in Figure 4. For $\Theta = 0$, the skyrmion transforms between the Néel ($\Phi = 0, \pi$) and Bloch ($\Phi = \pm\pi/2$) types, which are represented on the big toroidal circle. The antiskyrmions with diverse orientations ($\Theta = \pm\pi$) are located on the small toroidal circle. The two middle toroidal circles at the top and bottom represent various nonskyrmion states. Any toroidal circle route represents a skyrmion-number-invariant transformation. Any poloidal circle route on the torus describes the dynamic tuning between a Néel or Bloch skyrmion ($s = 1$) and an antiskyrmion ($s = -1$).

The skyrmion torus used to represent skyrmionic texture evolution has an intriguing relation to the orbital angular momentum (OAM) Poincaré sphere to represent the OAM evolution of a vortex beam. Using the methods introduced in the previous section, we can derive the parametric form of the corresponding vector beam as a function of Φ and Θ :

$$\Psi = \Psi_0 \mathbf{R} + [\cos(\Theta/2) e^{-i\Phi/2} \Psi_{-1} + \sin(\Theta/2) e^{i\Phi/2} \Psi_1] \mathbf{L} \quad (10)$$

where Ψ_0 is a zeroth-order Bessel (or fundamental Gaussian) mode and $\Psi_{\pm 1}$ are ± 1 -order Bessel modes (or LG modes)

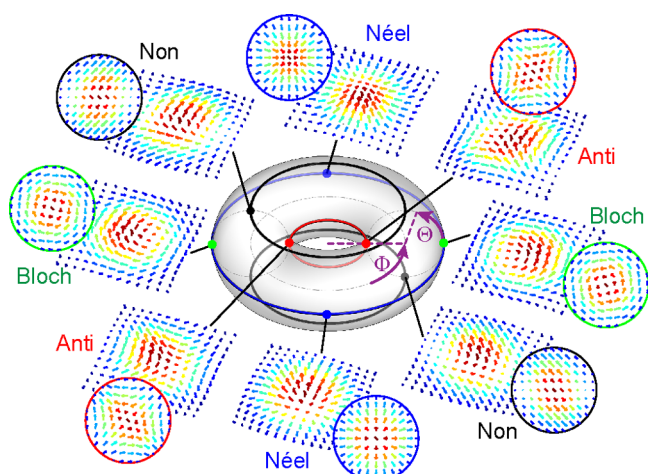


Figure 4. Skyrmion torus to represent the universal topological evolution of a tunable optical skyrmion, with special topologies as points on it: red points, Néel type; green points, Bloch type; blue points (the poles), antiskyrmion.

carrying opposite OAM with ± 1 topological charges. The spatial mode of the LCP component is exactly of the form of a conventional OAM Poincaré sphere,²⁶ driven by the longitude and latitude angles Φ and Θ , revealing the OAM conversion between ± 1 topological charges. In the OAM Poincaré sphere, when $\Theta = 0$, the scalar mode always represents an OAM with a single topological charge, independent of the value of Φ . This is why the OAM evolution is mapped on a sphere and the pure OAM state is represented on the pole. However, the skyrmionic vector beam adds a new degree of freedom to distinguish the Φ -dependent states with different Néel and Bloch textures when $\Theta = 0$. Thus, the combined skyrmionic vector texture should be mapped onto a torus. Therefore, the torus mapping acts as a useful tool to tailor general skyrmionic topological transformations, akin to the Poincaré sphere for tailoring OAM. Hence, many related applications, such as spin–orbit conversion, geometric phase transition, encoding, and communication,^{25,27,28} are expected to be analogously studied in optical skyrmions.

EXPERIMENT

In order to realize tunable optical skyrmions experimentally, we implemented a highly stable optical setup capable of generating arbitrary optical beams with almost any state of polarization and spatial profile,²⁹ which is shown schematically in Figure 5. This optical setup uses a spatial light modulator (SLM) for arbitrary control of the spatial distribution of the optical field.³⁰ The setup starts with a horizontally polarized HeNe (632.8 nm) laser beam, collimated and expanded to fully cover the liquid crystal screen of the SLM. The screen of the SLM is digitally split into two independent screens, each of which is addressed with an independent digital hologram that generates, in the first diffraction order, two independent optical fields. The holograms are chosen according to the desired skyrmion as given by eq 10. To better approximate the Bessel or LG modes, we modulated both the amplitude and phase of the desired modes using complex amplitude modulation (see ref 30 for additional details). For example, to generate skyrmions ($\Theta = 0$), only the second term of the LCP component is present, i.e., Ψ_1 . Hence, on one side of the SLM we encode the mode Ψ_0 the (fundamental Gaussian mode)

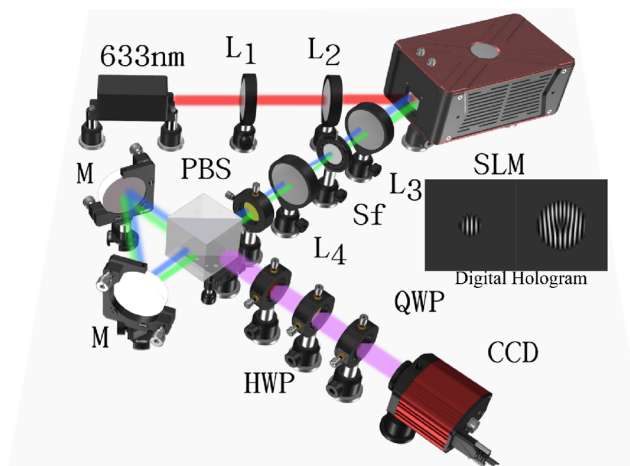


Figure 5. Schematic representation of the optical setup implemented to generate tunable optical skyrmions. L_1 – L_4 , lenses; PBS, polarizing beam splitter; SLM: spatial light modulator; HWP, half-wave plate; QWP, quarter-wave plate; M, mirror; Sf, spatial filter; CCD: charge-coupled device camera.

and on the other side the mode Ψ_1 (first-order Bessel or LG mode). An example of the encoded hologram is shown as an inset in Figure 5. It can also be seen here that each hologram is superimposed with a linear grating to separate the different diffraction orders and filter the first diffraction using a telescope formed by two lenses and a spatial filter located in the focal plane of the first lens. The two optical fields are then redirected to a common-path triangular Sagnac interferometer comprising a polarizing beam splitter (PBS) and two mirrors. Prior to entering the interferometer, the two beams are rotated to a diagonal polarization state. In this way, when the two beams enter the interferometer after traversing the PBS, each of them is separated into two new beams with orthogonal linear polarization states (horizontal and vertical) traveling along opposite optical paths. After a round trip, all four beams exit the interferometer from the opposite side of the PBS, two with horizontal polarization and two with vertical. Finally, the horizontal polarization component of one of the beams is aligned coaxially with the vertical polarization component of the other beam. To improve the coaxial superposition, fine-tuning is performed digitally via the period of the linear gratings encoded on each digital hologram. Importantly, optical aberrations produced by the screen of the SLM, which is not perfectly flat, induce small deviations between the experimental and theoretical results. Nonetheless, such aberrations could be removed by adding a correction mask to the SLM. Such corrections lie beyond the scope of this article since our purpose is just to demonstrate the concept.

The experimental reconstruction of the optical skyrmions was achieved through Stokes polarimetry, more specifically, through the reconstruction of the Stokes parameters S_0 , S_1 , S_2 , and S_3 , which were computed from a set of intensity measurements. To this end, a second stage was built at the output port of the interferometer, where a series of phase retarders and a charge-coupled device camera (CCD) allowed measurement of the required intensities, from which the Stokes parameters were reconstructed using the relations

$$\begin{aligned} S_0 &= I_H + I_V & S_1 &= 2I_H - S_0 \\ S_2 &= 2I_D - S_0 & S_3 &= 2I_R - S_0 \end{aligned} \quad (11)$$

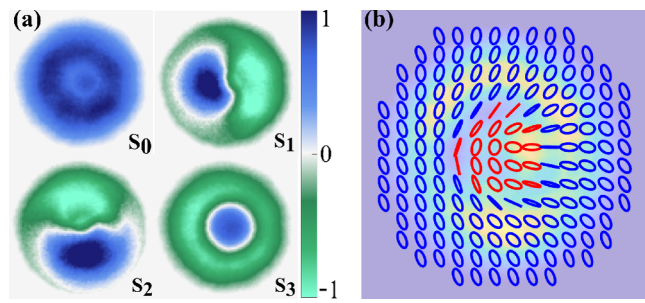


Figure 6. Experimentally reconstructed (a) Stokes parameters and (b) intensity distribution of the vector field overlapped with its corresponding polarization distribution.

where I_H , I_V , I_D , and I_R represent the intensities of the horizontal, vertical, diagonal, and RCP components, respectively. To experimentally measure I_H , I_V , and I_D we passed the optical field through a linear polarizer set at 0° , 45° , and 90° , respectively, while the intensity of the I_R polarization component was acquired by passing it simultaneously through a quarter-wave plate (QWP) at 45° and a linear polarizer at 90° (see ref 31 for further details). Figure 6a shows an example of the experimental Stokes parameters along with the intensity profile overlapped with its corresponding polarization distribution (Figure 6b) for the specific case $\phi_1 = \phi_2 = 0$. In this example, the beam center includes a pure RCP state ($S_3 = 1$), represented by a dark-blue color. This is the case because the beam is composed of a coaxial superposition of the LCP fundamental Gaussian mode and the LCP LG mode, which has a null at its center. Thus, the point in the center of the composed mode exists as a pure RCP ($S_3 = +1$) state, which exactly corresponds to a generic C-point.³² The holograms used in this example are displayed as insets in Figure 5 (digital hologram) and correspond from left to right to the fundamental Gaussian mode and the first-order LG mode. Importantly, all of the topological structures represented on the torus can be chosen according to eq 10 by simply changing the holograms displayed on the SLM.

With our digital hologram system, we realized the controlled generation of Stokes skyrmions with arbitrary topological textures on the skyrmion torus. Figure 7 shows our experimentally generated LG-based results for tunable Stokes skyrmions at typical points of the skyrmion torus, including the measured intensity and polarization distributions, Stokes vector fields, and a zoom-in of the central region of the vector field to clearly distinguish the topological textures. From our experimental results, we can clearly identify the textures (hedgehog for Néel-type skyrmion, vortex for Bloch-type skyrmion, and saddle for antiskyrmion). Importantly, the vector field shows a small experimental deviation from the theoretical predictions, but these errors can be tolerated since we are interested in the 3D topology of the skyrmionic structure, where no significant deviations are observed. For verification, we numerically calculated the skyrmion numbers of our experimental results using eq 1, and the results are noted in Figure 7. The experimental skyrmion numbers agree well with the corresponding theoretical predictions: antiskyrmions for $s = -1$ and Bloch- and Néel-type skyrmions for $s = 1$. Additional experimental results are shown in Videos S4 and S5 for the cases based on LG and Bessel–Gaussian modes.

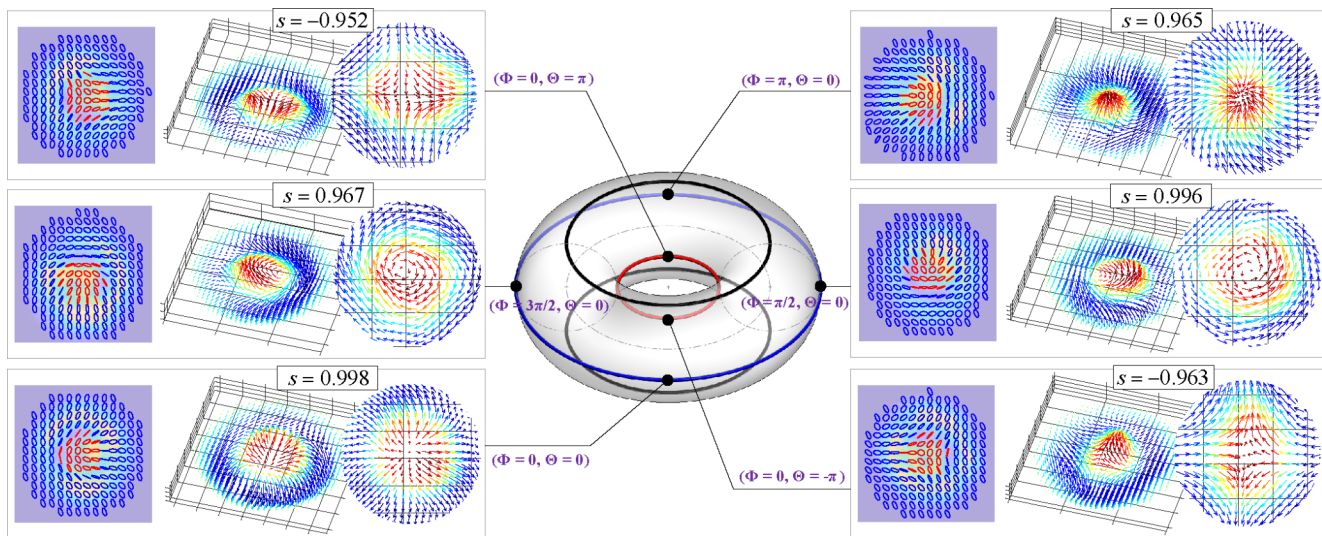


Figure 7. Experimental results for tunable Stokes skyrmions with controlled topological textures corresponding to selected points on the skyrmion torus, as shown in the gray boxes. Each box includes the measured intensity and polarization distribution of the skyrmionic beam, the vector distribution of the Stokes skyrmions, and the zoom-in plane form of the vector field to clearly distinguish the topological texture. Numerically calculated skyrmion numbers are noted in the diverse panels correspondingly.

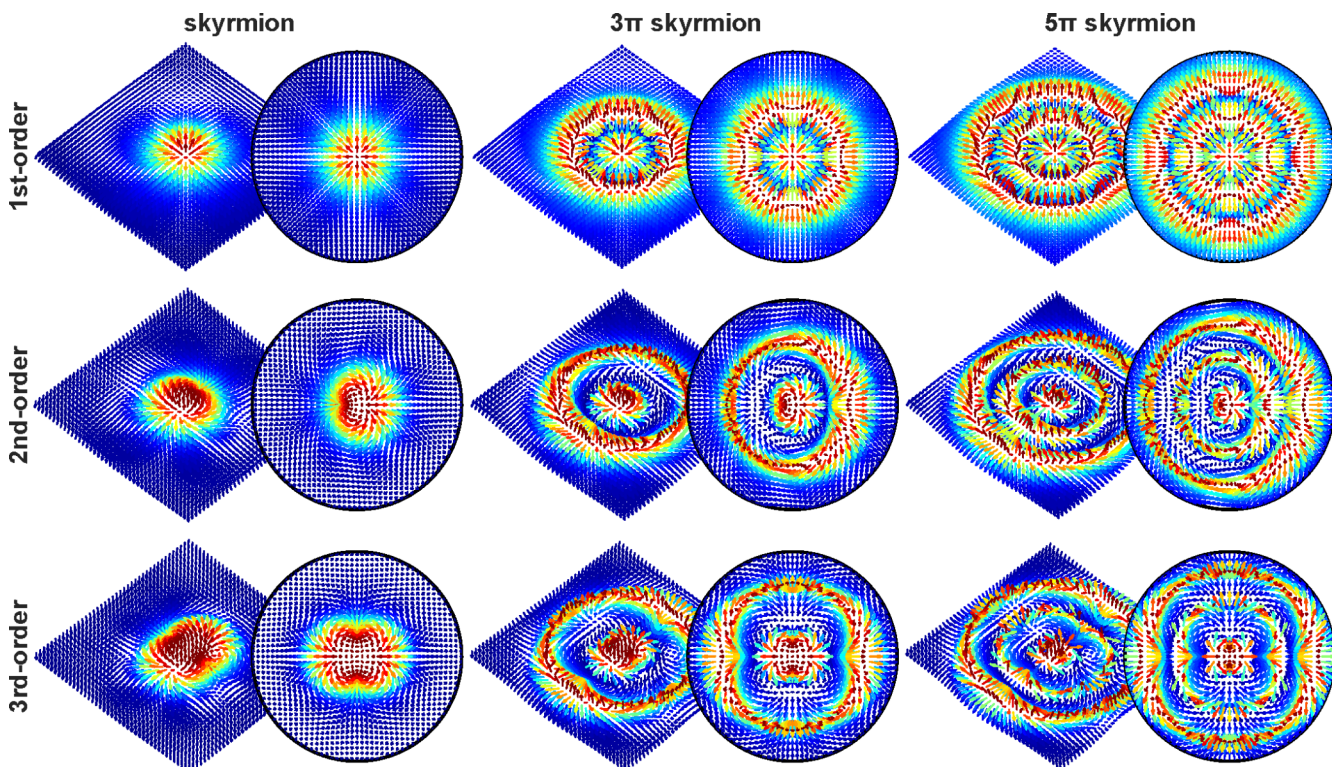


Figure 8. Theoretical results for complex higher-order $k\pi$ skyrmions in the Stokes vector field of the mode $\Psi_{p,l}$. The inset of each panel shows the corresponding transverse component distribution. The first, second, and third rows correspond to the results for vorticity numbers of 1, 2, and 3 for the parameter used as $l = 1, 2$, and 3, respectively. The first, second, and third columns correspond to the results for radial twists of 1π , 3π , and 5π for the parameter used as $p = 0, 1$, and 2, respectively.

DISCUSSION

Although the generalized tunable optical skyrmion model is inspired from the case of an SPP electric field and realized using a Stokes vector field, it is not limited to these cases and can be freely extendable. Because the new concept of a tunable skyrmion has a universal mathematical parametrization for a generalized topology, the vector can refer to other kinds of

optical fields of structured light for further exploration. For example, we can also use spin vectors in a tightly focused beam,^{4,5} electric or magnetic vectors in a propagating structured pulse,⁸ and pseudospins in nonlinear media.⁹ It is also an exciting direction to create more quasiparticles with complex topological states beyond skyrmions, such as skyrmion bags³³ and skyrmion tubes³⁴ as well as merons and bimerons,^{35–37} into structured light. Even though in this work

we used an SLM to generate skyrmionic beams, digital mirror devices are an alternative means to generate them that present several advantages over SLMs, such as their high refresh rates, polarization independence, and low cost.³¹

The above results show only cases with skyrmion numbers of ± 1 . Nonetheless, our model can be easily extended to higher-order skyrmions with increasingly complex topologies that are hard to realize with previous optical skyrmions methods. To this end, we need only to replace the single-topological-charge vortex mode Ψ_{\pm} in eq 10 with general LG modes with both radial and azimuthal indices $\psi_{p,l}$:

$$\Psi_{p,l} = \psi_{0,0}\mathbf{R} + [\cos(\Theta/2) e^{-i\Phi/2}\psi_{p,-l} + \sin(\Theta/2) e^{i\Phi/2}\psi_{p,l}]\mathbf{L} \quad (12)$$

This equation represents more general topological skyrmions in its Stokes fields. The index p controls the radial multitwist structure of the skyrmion, i.e., the so-called skyrmionium or $k\pi$ target skyrmion,³⁸ and the index l controls higher vorticity numbers in the skyrmion, i.e., the structures previously called higher-order skyrmions.⁹ A set of results for Néel-type complex higher-order $k\pi$ skyrmions based on eq 12 are shown in Figure 8.

It is worth mentioning that even though the skyrmions studied in this work share some similarities with full Poincaré beams^{39–42} and their associated polarization singularities,^{32,43} there are clear differences. Thus, it is worth unveiling the relationship between the new concept of tunable topological skyrmions and Poincaré beams. For instance, the Néel-to-Bloch skyrmion corresponds to a Poincaré beam with a lemon-type C-point, whereas an antiskyrmion corresponds to a start-type C-point. Therefore, it is still interesting to study the relationship between other kinds of complex skyrmions and Poincaré beams with polarization singularities.

Finally, even though proposing novel techniques for the generation of diverse topological skyrmions is of great relevance, another interesting direction would be a study of novel techniques for the characterization of such structures. More precisely, for a given skyrmionic beam, it is desired to precisely quantify its topological state on the skyrmion torus with coordinates (Φ, Θ) . We can anticipate that some recent advanced measurement methods for vector beams, such as the state tomography method,⁴⁴ represent a promising avenue for this.

CONCLUSION

We have proposed an extended family of tunable optical skyrmions enabling flexible transformations among various kinds of skyrmionic topological textures. A graphical model, the skyrmion torus, is proposed to universally represent the topological evolution of tunable optical skyrmions. We experimentally generated such tunable optical skyrmions in Stokes vector fields of customized vector beams from a well-designed digital hologram system. This is the first known experimental generation of topology-tunable optical skyrmions in free space and also the first realization of optical antiskyrmions. Our methods could easily be extended to higher-order topologies to provide a new platform for optical information storage, communication, and cryptography using skyrmionic topological states of light.

Finally, it has come to our attention that when we were preparing this article, an independent experiment that explored optical skyrmions in a vector beam was reported.⁴⁵ It focused

on a 3D skyrmion structure, while we have focused on the tunability of 2D skyrmion structures. In contrast to conventional 2D skyrmions (with spin textures confined to a 2D plane), the 3D skyrmion, as a generalized form, can include multiple topological textures in multiple transverse planes upon propagation. Therefore, it is also a meaningful future direction to improve our approach to control topologically tunable 3D skyrmions.

ASSOCIATED CONTENT

Supporting Information

The Supporting Information is available free of charge at <https://pubs.acs.org/doi/10.1021/acsphtronics.1c01703>.

Video S1: Topology-tunable skyrmion transformed between Néel- and Bloch-types ([MP4](#))

Video S2: Topology-tunable skyrmion transformed between Bloch- and Antitypes ([MP4](#))

Video S3: Topology-tunable skyrmion transformed between Néel- and Antitypes ([MP4](#))

Video S4: Experimental results of topology-tunable skyrmion controlled on skyrmion torus based on an LG mode ([MP4](#))

Video S5: Experimental results of topology-tunable skyrmion controlled on skyrmion torus based on a Bessel–Gaussian mode ([MP4](#))

AUTHOR INFORMATION

Corresponding Authors

Yijie Shen – Optoelectronics Research Centre and Centre for Photonic Metamaterials, University of Southampton, Southampton SO17 1BJ, United Kingdom;  orcid.org/0000-0002-6700-9902; Email: y.shen@soton.ac.uk

Carmelo Rosales-Guzmán – Centro de Investigaciones en Óptica, A. C., 37150 León, Gto., México; Wang Da-Heng Collaborative Innovation Center for Quantum Manipulation and Control, Harbin University of Science and Technology, Harbin 150080, China; Optoelectronics Research Centre and Centre for Photonic Metamaterials, University of Southampton, Southampton SO17 1BJ, United Kingdom; Email: carmelorosalesg@cio.mx

Author

Eduardo Casas Martínez – Departamento de Óptica, Instituto Nacional de Astrofísica, Óptica y Electrónica, 72000 Puebla, México

Complete contact information is available at: <https://pubs.acs.org/10.1021/acsphtronics.1c01703>

Notes

The authors declare no competing financial interest.

ACKNOWLEDGMENTS

This work was supported by the National Natural Science Foundation of China (grant nos. 61975047 and 11934013) and the High-Level Talents Project of Heilongjiang Province (grant no. 2020GSP12).

REFERENCES

- (1) Göbel, B.; Mertig, I.; Tretiakov, O. A. Beyond skyrmions: Review and perspectives of alternative magnetic quasiparticles. *Phys. Rep.* **2021**, *895*, 1–28.

- (2) Fert, A.; Reyren, N.; Cros, V. Magnetic skyrmions: advances in physics and potential applications. *Nat. Rev. Mater.* **2017**, *2*, 17031.
- (3) Tsesses, S.; Ostrovsky, E.; Cohen, K.; Gjonaj, B.; Lindner, N. H.; Bartal, G. Optical skyrmion lattice in evanescent electromagnetic fields. *Science* **2018**, *361*, 993–996.
- (4) Du, L.; Yang, A.; Zayats, A. V.; Yuan, X. Deep-subwavelength features of photonic skyrmions in a confined electromagnetic field with orbital angular momentum. *Nat. Phys.* **2019**, *15*, 650–654.
- (5) Gutiérrez-Cuevas, R.; Pisanty, E. Optical polarization skyrmionic fields in free space. *J. Opt.* **2021**, *23*, 024004.
- (6) Gao, S.; Speirits, F. C.; Castellucci, F.; Franke-Arnold, S.; Barnett, S. M.; Götte, J. B. Paraxial skyrmionic beams. *Phys. Rev. A* **2020**, *102*, 053513.
- (7) Lin, W.; Ota, Y.; Arakawa, Y.; Iwamoto, S. Microcavity-based generation of full Poincaré beams with arbitrary skyrmion numbers. *Phys. Rev. Res.* **2021**, *3*, 023055.
- (8) Shen, Y.; Hou, Y.; Papasimakis, N.; Zheludev, N. I. Supertoroidal light pulses as electromagnetic skyrmions propagating in free space. *Nat. Commun.* **2021**, *12*, 5891.
- (9) Karnieli, A.; Tsesses, S.; Bartal, G.; Arie, A. Emulating spin transport with nonlinear optics, from high-order skyrmions to the topological Hall effect. *Nat. Commun.* **2021**, *12*, 1092.
- (10) Dai, Y.; Zhou, Z.; Ghosh, A.; Mong, R. S. K.; Kubo, A.; Huang, C.-B.; Petek, H. Plasmonic topological quasiparticle on the nanometre and femtosecond scales. *Nature* **2020**, *588*, 616–619.
- (11) Davis, T. J.; Janoschka, D.; Dreher, P.; Frank, B.; Meyer zu Heringdorf, F.-J.; Giessen, H. Ultrafast vector imaging of plasmonic skyrmion dynamics with deep subwavelength resolution. *Science* **2020**, *368*, eaba6415.
- (12) Yu, X. Z.; Onose, Y.; Kanazawa, N.; Park, J. H.; Han, J. H.; Matsui, Y.; Nagaosa, N.; Tokura, Y. Real-space observation of a two-dimensional skyrmion crystal. *Nature* **2010**, *465*, 901–904.
- (13) Nagaosa, N.; Tokura, Y. Topological properties and dynamics of magnetic skyrmions. *Nat. Nanotechnol.* **2013**, *8*, 899–911.
- (14) Kézsmárki, I.; Bordács, S.; Milde, P.; Neuber, E.; Eng, L. M.; White, J. S.; Rønnow, H. M.; Dewhurst, C. D.; Mochizuki, M.; Yanai, K.; Nakamura, H.; Ehlers, D.; Tsurkan, V.; Loidl, A. Néel-type skyrmion lattice with confined orientation in the polar magnetic semiconductor gallium arsenide. *Nat. Mater.* **2015**, *14*, 1116–1122.
- (15) Gilbert, D. A.; Maranville, B. B.; Balk, A. L.; Kirby, B. J.; Fischer, P.; Pierce, D. T.; Unguris, J.; Borchers, J. A.; Liu, K. Realization of ground-state artificial skyrmion lattices at room temperature. *Nat. Commun.* **2015**, *6*, 8462.
- (16) Nayak, A. K.; Kumar, V.; Ma, T.; Werner, P.; Pippel, E.; Sahoo, R.; Damay, F.; Rößler, U. K.; Felser, C.; Parkin, S. S. P. Magnetic antiskyrmions above room temperature in tetragonal Heusler materials. *Nature* **2017**, *548*, 561–566.
- (17) Bai, C.; Chen, J.; Zhang, Y.; Zhang, D.; Zhan, Q. Dynamic tailoring of an optical skyrmion lattice in surface plasmon polaritons. *Opt. Express* **2020**, *28*, 10320–10328.
- (18) Meiler, T.; Frank, B.; Giessen, H. Dynamic tailoring of an optical skyrmion lattice in surface plasmon polaritons: comment. *Opt. Express* **2020**, *28*, 33614–33615.
- (19) Bai, C.; Chen, J.; Zhang, D.; Zhan, Q. Dynamic tailoring of an optical skyrmion lattice in surface plasmon polaritons: reply. *Opt. Express* **2020**, *28*, 33616–33618.
- (20) Zhang, Q.; Xie, Z.; Du, L.; Shi, P.; Yuan, X. Bloch-type photonic skyrmions in optical chiral multilayers. *Phys. Rev. Res.* **2021**, *3*, 023109.
- (21) Yu, X. Z.; Koshiba, W.; Tokunaga, Y.; Shibata, K.; Taguchi, Y.; Nagaosa, N.; Tokura, Y. Transformation between Meron and skyrmion topological spin textures in a chiral magnet. *Nature* **2018**, *564*, 95–98.
- (22) Jani, H.; Lin, J.-C.; Chen, J.; Harrison, J.; Maccherozzi, F.; Schad, J.; Prakash, S.; Eom, C.-B.; Ariando, A.; Venkatesan, T.; Radaelli, P. G. Antiferromagnetic half-skyrmions and bimerons at room temperature. *Nature* **2021**, *590*, 74–79.
- (23) Xiong, L.; Li, Y.; Halbertal, D.; Sammon, M.; Sun, Z.; Liu, S.; Edgar, J. H.; Low, T.; Fogler, M. M.; Dean, C. R.; Millis, A. J.; Basov, D. N. Polaritonic vortices with a half-integer charge. *Nano Lett.* **2021**, *21*, 9256–9261.
- (24) Wang, X. S.; Yuan, H. Y.; Wang, X. R. A theory on skyrmion size. *Commun. Phys.* **2018**, *1*, 31.
- (25) Rosales-Guzmán, C.; Ndagano, B.; Forbes, A. A review of complex vector light fields and their applications. *J. Opt.* **2018**, *20*, 123001.
- (26) Padgett, M. J.; Courtial, J. Poincaré-sphere equivalent for light beams containing orbital angular momentum. *Opt. Lett.* **1999**, *24*, 430–432.
- (27) Shen, Y.; Wang, X.; Xie, Z.; Min, C.; Fu, X.; Liu, Q.; Gong, M.; Yuan, X. Optical vortices 30 years on: OAM manipulation from topological charge to multiple singularities. *Light: Sci. Appl.* **2019**, *8*, 90.
- (28) Dennis, M. R.; Alonso, M. A. Swings and roundabouts: optical Poincaré spheres for polarization and Gaussian beams. *Philos. Trans. R. Soc. A* **2017**, *375*, 20150441.
- (29) Perez-Garcia, B.; López-Mariscal, C.; Hernandez-Aranda, R. I.; Gutiérrez-Vega, J. C. On-demand tailored vector beams. *Appl. Opt.* **2017**, *56*, 6967–6972.
- (30) Rosales-Guzmán, C.; Forbes, A. *How to Shape Light with Spatial Light Modulators*; SPIE Press, 2017; p 57.
- (31) Rosales-Guzmán, C.; Hu, X.-B.; Selyem, A.; Moreno-Acosta, P.; Franke-Arnold, S.; Ramos-García, R.; Forbes, A. Polarisation-insensitive generation of complex vector modes from a digital micromirror device. *Sci. Rep.* **2020**, *10*, 10434.
- (32) Otte, E.; Denz, C. Customization and analysis of structured singular light fields. *J. Opt.* **2021**, *23*, 073501.
- (33) Foster, D.; Kind, C.; Ackerman, P. J.; Tai, J.-S. B.; Dennis, M. R.; Smalyukh, I. I. Two-dimensional skyrmion bags in liquid crystals and ferromagnets. *Nat. Phys.* **2019**, *15*, 655–659.
- (34) Kuratsuji, H.; Tsuchida, S. Evolution of the stokes parameters, polarization singularities, and optical skyrmion. *Phys. Rev. A* **2021**, *103*, 023514.
- (35) Shen, Y. Topological bimeronic beams. *Opt. Lett.* **2021**, *46*, 3737.
- (36) Król, M.; Sigurdsson, H.; Rechcińska, K.; Oliwa, P.; Tyszka, K.; Bardyzewski, W.; Opala, A.; Matuszewski, M.; Morawiak, P.; Mazur, R.; Piecik, W.; Kula, P.; Lagoudakis, P. G.; Piętka, B.; Szczętko, J. Observation of second-order Meron polarization textures in optical microcavities. *Optica* **2021**, *8*, 255–261.
- (37) Guo, C.; Xiao, M.; Guo, Y.; Yuan, L.; Fan, S. Meron spin textures in momentum space. *Phys. Rev. Lett.* **2020**, *124*, 106103.
- (38) Song, C.; Ma, Y.; Jin, C.; Wang, J.; Xia, H.; Wang, J.; Liu, Q. Field-tuned spin excitation spectrum of $k\pi$ skyrmion. *New J. Phys.* **2019**, *21*, 083006.
- (39) Beckley, A. M.; Brown, T. G.; Alonso, M. A. Full poincaré beams. *Opt. Express* **2010**, *18*, 10777–10785.
- (40) Ling, X.; Yi, X.; Dai, Z.; Wang, Y.; Chen, L. Characterization and manipulation of full Poincaré beams on the hybrid Poincaré sphere. *J. Opt. Soc. Am. B* **2016**, *33*, 2172–2176.
- (41) Donati, S.; Dominici, L.; Dagvadorj, G.; Ballarini, D.; De Giorgi, M.; Bramati, A.; Gigli, G.; Rubo, Y. G.; Szymańska, M. H.; Sanvitto, D. Twist of generalized skyrmions and spin vortices in a polariton superfluid. *Proc. Natl. Acad. Sci. U.S.A.* **2016**, *113*, 14926–14931.
- (42) Lopez-Mago, D. On the overall polarisation properties of Poincaré beams. *J. Opt.* **2019**, *21*, 115605.
- (43) Otte, E.; Alpmann, C.; Denz, C. Polarization singularity explosions in tailored light fields. *Laser Photonics Rev.* **2018**, *12*, 1700200.
- (44) Toninelli, E.; Ndagano, B.; Vallés, A.; Sephton, B.; Nape, I.; Ambrosio, A.; Capasso, F.; Padgett, M. J.; Forbes, A. Concepts in quantum state tomography and classical implementation with intense light: a tutorial. *Adv. Opt. Photonics* **2019**, *11*, 67–134.
- (45) Susic, D.; Droop, R.; Otte, E.; Ehrmantraut, D.; Nori, F.; Ruostekoski, J.; Denz, C.; Dennis, M. R. Particle-like topologies in light. *Nat. Commun.* **2021**, *12*, 6785.